Supporting Information

Achieving Reproducibility and High Efficiency (>21%) Perovskite Solar Cells with a Pre-synthesized $FAPbI_3$ Powder

Yong Zhang,[†] Seongrok Seo,[⊥] Soo Yeon Lim,[§] Younghoon Kim,[⊥] Seul-Gi Kim,[†] Do-Kyoung Lee,[†] Sun-Ho Lee,[†] Hyunjung Shin,[⊥] Hyeonsik Cheong,[§] and Nam-Gyu Park[*,†]*

[†]School of Chemical Engineering, Sungkyunkwan University, Suwon 16419, Korea

[⊥]Department of Energy Science, Sungkyunkwan University, Suwon 16419, Korea

[§]Department of Physics, Sogang University, Seoul 04107, Korea

*Corresponding author email: npark@skku.edu

Experimental Section

Materials. Colloidal tin oxide solution (SnO_2, 15% in H_2O) was purchased from Alfa Aesar. Methylamine (40% in methanol, *ca*. 9.8 mol/L) was purchased from TCI. Potassium iodide (anhydrous, 99%), lead(II) nitrate (ACS reagent, ≥99%), acetic acid (>99%), formamidine acetate (99%), hydriodic acid (contains no stabilizer, distilled, 57 wt.% in H_2O, 99.99% trace metals basis), hydrochloric acid (ACS reagent, 37%), *N,N*-dimethylformamide (anhydrous, 99.8%), dimethyl sulfoxide (anhydrous, ≥99.9%), chlorobenzene (anhydrous, 99.8%), diethyl ether (contains 1 ppm BHT as inhibitor, anhydrous, ≥99.7%) and 4-*tert*-butylpyridine (98%) were purchased from Sigma-Aldrich. Spiro-MeOTAD was purchased from Merck. PbI_2 (95%) for powder synthesis was purchased from Kanto Chemical Co., Inc. Acetonitrile (HPLC) for the powder synthesis was purchased from DeaJung Chemicals. All the purchased chemicals were used as received without further purification.

Synthesis of PbI_2. Lead iodide (PbI_2) was synthesized by reacting KI with $Pb(NO_3)_2$, where the aqueous

KI solution (23.2 g KI in deionized water (DI water)) and the aqueous $Pb(NO_3)_2$ solution (33.1 g $Pb(NO_3)_2$ in DI water) were mixed with vigorous stirring at room temperature for 4 h, which was followed by adding acetic acid (20 mL) and additional DI water (2 L) and then heated at 90 °C for more than 24 h. The supernatant liquid was removed, and the precipitate was recrystallized by cooling down. The recrystallized golden crystals were filtered and rinsed with DI water several times. Finally, the product was dried at 85 °C in a vacuum oven for 24 h and then stored in Ar filled glove box.

Synthesis of FAI and MACl. Formamidinium iodide (FAI, $HC(NH_2)_2I$) was synthesized by reacting 15 g of formamidinium acetate with 30 mL of hydroiodic acid in a round-bottomed flask in an ice bath for 2 h. Dark yellow precipitate was recovered by evaporating at 60 ºC for 1 h. Resulting product was dissolved in ethanol and recrystallized in diethyl ether, which was repeated for three times. methylammonium chloride (MACl, CH_3NH_3Cl) was synthesized using methylamine and hydrochloric acid in a similar way with FAI. The final white precipitates were dried at 50 °C in a vacuum oven for 24 h and then stored in Ar filled glove box.

Synthesis of $FAPbI_3$ powder. For $FAPbI_3$ powder synthesis, 7.66 g of FAI was added into Erlenmeyer flask containing 150 mL acetonitrile (ACN) under vigorous stirring and then the synthesized PbI_2 or low-grade (95% purity) commercial PbI_2 (15.67 g) (PbI_2:FAI = 1:1.3) was slowly added together with extra 50 mL ACN. The brown precipitate appeared after addition of PbI_2. After vigorous stirring for 24 h, the powder turned gradually bright yellow. Then the powder was washed with ACN and diethyl ether for six times. The final product was dried in a vacuum oven for 24 h and then stored in Ar filled glove box. The yield was 93%. (*Caution: in case of scale-up, rotary evaporator is recommended to dry the powder instead of using a vacuum oven.*). The $FAPbI_3$ powder is also commercially available

from ShareChem Co., Ltd.

Solar cell fabrication. F-doped tin oxide (FTO) coated conductive glasses (T18VU70, 12-13 Ω/sq, AGC Fabritech Co., Ltd.) were cleaned by detergent, followed by ultrasonic treatment in ethanol for 20 min. UV/ozone (UVO) treatment was conducted for 60 min prior to use. SnO_2 film was deposited on the FTO substrate by spin-coating the commercial SnO_2 colloidal solution (diluted with DI water to adjust to 4 wt%) at 4000 rpm for 20 s, which was annealed at 185 °C on a hotplate for 30 min. The $FAPbI_3$ perovskite precursor solution was prepared by mixing 663 mg of the synthesized $FAPbI_3$ powder and 71 μL of DMSO (molar ratio 1:1) in 568 μL of DMF with different molar ratio (0 mol%, 10 mol%, 20 mol%, 30 mol% and 40 mol%) of MACl (optimal was 20 mol%). For the conventional precursor mixture solution, except for using the synthesized powder, PbI_2 (Alfa Aesar, 99.9985%) and the synthesized FAI were dissolved. The solution was spin-coated at two consecutive steps of 1000 rpm for 5 and 5000 rpm 20 s. During the second spin-coating step, 1 mL of diethyl ether was quickly dripped on the rotating substrate (5000 rpm) at 17 s to obtain an adduct intermediate film. The adduct films were annealed at 150 °C on a hotplate for 10 min. The spiro-MeOTAD layer was formed on the perovskite layer by spin-coating of 20 μL of the stock solution comprising 50 mg spiro-MeOTAD in 0.55 mL chlorobenzene including 19.5 μL t-BP (tert-butylpyridine) and 11.5 μL Li-TFSI solution (540 mg Li-TFSI in 1 mL acetonitrile (Sigma-Aldrich, 99.8%)) at 3000 rpm for 30 s. Finally, Ag electrode with a thickness of ca. 150 nm was deposited on top of the spiro-MeOTAD layer under 4×10^{-7} torr using a thermal evaporator. The as-fabricated PSCs were stored in the desiccator overnight before the current density-voltage (J-V) measurement.

Characterizations. J-V curves were recorded using a Keithley 2400 source meter under the simulated

one sun illumination (AM 1.5G, 100 mW/cm^2) using a solar simulator (Oriel Sol 3A class AAA) equipped with 450 W Xenon lamp (Newport 6280NS), in which light intensity was adjusted by NREL-calibrated Si solar cell with KG-2 filter. Solar cells were covered with a metal mask with an aperture area of 0.125 cm^2 during the measurement. External quantum efficiency (EQE) was measured by either an EQE system (PV measurement Inc.) equipped with a 75 W Xenon source lamp (USHIO, Japan) or a QuantX-300 Quantum Efficiency System (Newport) equipped with 100 W Xenon lamp. EQE data were collected at DC mode without bias light. The absorbance of the perovskite film was measured by UV-vis spectrometer (Lambda 45, Perkin-Elmer).

Steady-state photoluminescence (PL) was measured using a fluorescence spectrometer (Quantaurus-Tau C11367-12, Hamamatsu). Perovskite films were photo-excited with a 464 nm laser pulsed at the frequency of 10 MHz. The PL was detected by high sensitivity photon counting near-IR detector. Time-resolved photoluminescence (TRPL) spectra were measured using a time-correlated single photon counting (TCSPC) system by FluoTim 200 (PicoQuant) with 500 kHz repetition rate. The perovskite films were excited by 375 nm laser source, and then the emitted PL from the samples was collected by a photon multiplier tube (PMT) detector (PMA 182, PicoQuant-GmbH) at 800 nm.

X-ray diffraction (XRD) and grazing incidence X-ray diffraction (GIXRD) data were collected from a Rigaku SmartLab diffractometer, where Cu Kα radiation was used (λ = 1.5406 Å) and a scan rate was 4º/min with 0.02º/step. GIXRD were measured with the incident angle of 1º, 2º, 3º and 4º in the range of 5º - 40º with 0.01º/step. The GIXRD penetration depth depending on incidence angles was calculated from eq 1,[1]

$$\tau_{1/e} = \sin \theta/\mu \quad (1)$$

where $\tau_{1/e}$ is the depth at which the intensity of radiation on a material is attenuated to 1/e (37%) and μ is the linear absorption coefficient, $\mu = \mu_m\rho$ (μ_m is the mass absorption coefficient and ρ is the mass density). ρ for cubic unit cell crystal structure could be calculated using eq 2,

$$\rho = M/(a^3 \times N_A) \quad (2)$$

where M is the molar mass of $FAPbI_3$ (632.98 g/mol), N_A is Avogadro's number (6.022×10^{23}), a is the edge length of unit cell (a = 6.35694 Å for cubic $FAPbI_3$ determined from XRD analysis). The mass density ρ was calculated to be 4.092 g/cm^3. According to the NIST standard reference database,[2] the μ_m of $FAPbI_3$ is 246.9 cm^2/g at 8000 eV photo energy. According to the eq 1, the penetration depth $\tau_{1/e}$ of $FAPbI_3$ under incidence angle of 1°, 2°, 3°, 4°and 5° are 172.7 nm, 345.4 nm, 518.0 nm, 690.5 nm and 862.7 nm, respectively.

Light-intensity-dependent photocurrent mappings (PCM) were obtained using an atomic force microscope (AFM, NX10, Park System) equipped with a white LED light source (maximum power: 3.3 W), where light intensity was modulated from 0% (dark) to 20% (0.66 W), 40% (1.32 W), 60% (1.98 W) and 80% (2.64 W). The sub-mode of the PCM was Variable-Enhanced Conductive AFM (VECA) using the cantilever (SD-CDTP-NCHR) and 1 V DC bias voltage was applied to the substrate. The current images were obtained under the ambient condition.

The depth profile of the perovskite film on FTO substrate was recorded using time-of-flight secondary ion mass spectrometry (TOF-SIMS, model TOF-SIMS 5 of ION-TOF, Germany) in negative polarity. The pulsed primary Bi^+ ion source was operated at 25 keV and pA scale on a 40 μm × 40 μm area to bombard the sample surface to produce secondary ions. The sputtering was performed with a Cs^+ ion

beam operated at 1 keV and 45 nA on a 150 μm × 150 μm area.

Defect density was estimated using hole-only devices with the structure of FTO/PEDOT:PSS/perovskite/spiro-MeOTAD/Au. The devices were measured from -0.1 V to 2 V in the dark. The observed response was analyzed according to space-charge-limited current (SCLC) theory. Defect density ($N_{defects}$) was estimated using the relation $V_{TFL} = eN_{defects}d^2/2\varepsilon_r\varepsilon_0$,[3] where V_{TFL} is the trap-filled-limit voltage, e is electron charge (1.602×10^{-19} C), ε_r is relative dielectric constant, ε_0 is the vacuum permittivity (8.8542×10^{-14} F/cm) and d is the perovskite film thickness. The dielectric constant was calculated using the equation of $\varepsilon_r = Cd/A\varepsilon_0$, where C is capacitance at high frequency (~10^4 Hz) and A is area.[4,5]

Raman spectra were collected in back-scattering geometry. The 514.5 nm (2.41 eV) line of an Ar ion laser was used as an excitation source. The laser beam was focused on the surface of the solution in a petri-dish by a 50× microscope objective lens (0.8 NA). The scattered light was collected and collimated by the same objective in the backscattering geometry. The scattered signal was dispersed by a Jobin-Yvon Horiba iHR550 spectrometer (2400 grooves/mm) and detected with a liquid-nitrogen-cooled back-illuminated charge-coupled-device (CCD) detector. To approach the low-frequency range below 100 cm^{-1}, volume holographic filters (Optigrate) were used to clean the laser line and reject the Rayleigh-scattered light. The laser power was kept below 100 μW in order to avoid local heating.

Surface and cross-sectional morphologies were investigated by scanning electron microscope (SEM) (JSM-7600F, JEOL). Absorption spectra were measured using an UV/visible spectrometer (Lambda 45, Perkin Elmer).

Transmission electron microscopy (TEM) images and selected area electron diffraction (SAED) patterns of the cross-sectioned full cells were obtained using a high-resolution transmission electron microscope (JEOL JEM-2100F) at an acceleration voltage 200 kV. The specimens for TEM were prepared by vertical etching using focused ion beam (FIB) equipment (JEOL JIB-4601F) with the cell structure glass/FTO/SnO_2/perovskite/spiro-MeOTAD. Before preparing the specimens, Pt and carbon layers were deposited on the spiro-MeOTAD layer to protect the samples from milling damage. A thick plate was extracted from the bulk sample at 30 kV and 3,000~30,000 pA, which was welded on Cu grid (omniprobe grid) by using probing system. The thick plate was first thinned at 30 kV and 50~1,000 pA and then lower current of 10~30 pA. Finally, the specimen was completed by thinning at lower voltage of 1 kV and 30~50 pA after beam showering at 3 kV and 10~30 pA.

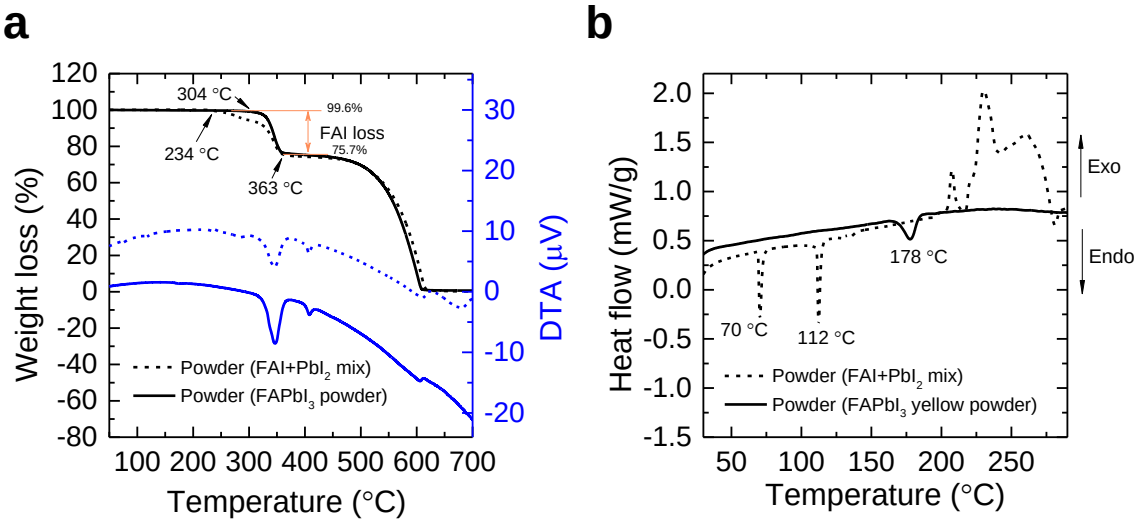

Figure S1. Thermogravimetric analysis (TGA) and differential scanning calorimetry (DSC) obtained at heating rate of 10 °C/min under N_2 atmosphere. (a) TGA along with DTA and (b) DSC for the conventional PbI_2 and FAI precursor mixture and the synthesized $FAPbI_3$ powder.

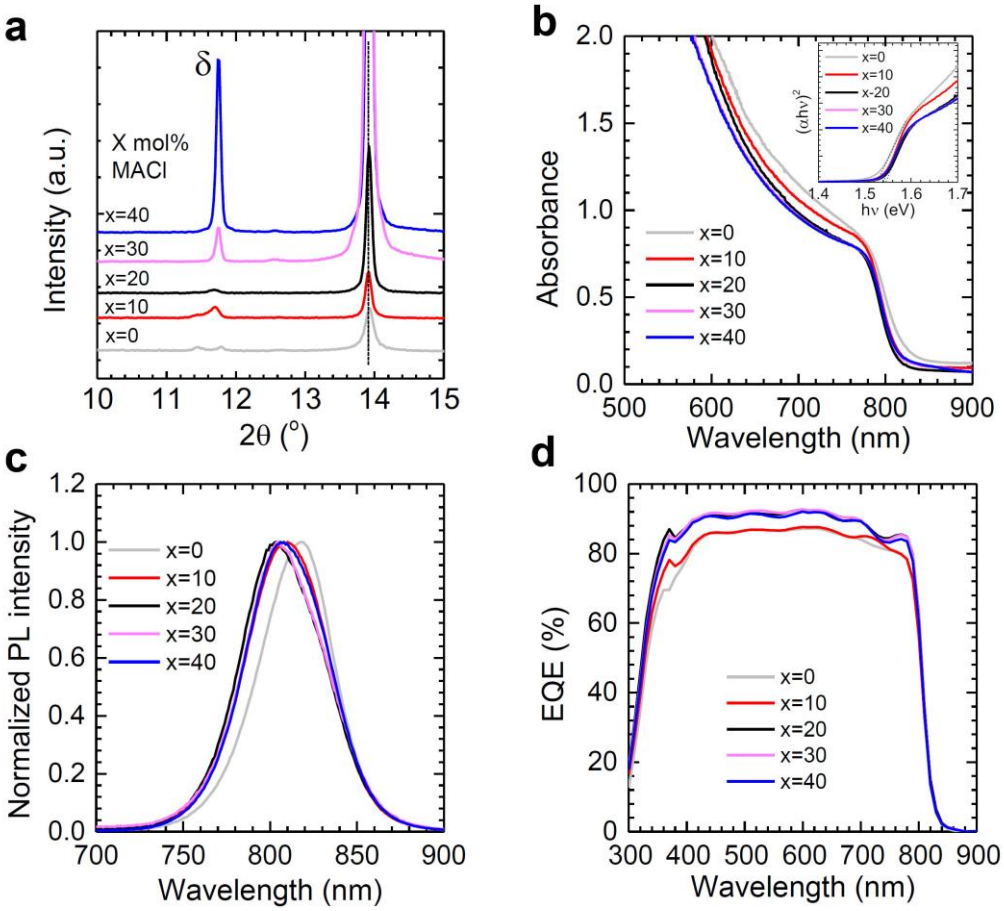

Figure S2. Effect of MACl content in the $FAPbI_3$ powder on structural, optical and EQE properties of $FAPbI_3$ films. (a) X-ray diffraction (XRD) patterns. (b) UV-vis absorption spectra (insert is Tauc plot). (c) Steady-state PL. The excitation wavelength was 464 nm for PL. (d) External quantum efficiency (EQE) of PSCs. For XRD in (a), data were obtained after exposing the annealed $FAPbI_3$ films for 15 h in relative humidity of about 50%. Peaks at 11.7° for 10-40 mol% correspond to δ phase, while δ phase appears at 11.4° without MACl.

Note for Figure S2. Different molar ratio (0 mol%, 10 mol%, 20 mol%, 30 mol% and 40 mol%) of MACl were added into the perovskite precursor solution to fabricate the perovskite film. From the XRD pattern in Figure S2a, the peaks at 11.7° correspond to δ-phase, where the 20 mol% MACl doped perovskite film shows almost no δ-phase. The appearance of δ-phase is indicative of degradation due to α → δ phase transition under humidity condition (fresh samples did not show δ-phase). Thus the suppression of δ-phase for the 20 mol% MACl doped perovskite film indicates that α-phase is relatively stable for this content. The (100) peak position at 13.92° for α-phase $FAPbI_3$ is not altered by the MACl content, which indicates that MA ion might not be involved in the crystal lattice. However,

in Figure S2b and S2c of the UV-vis absorption and PL spectra, the PL peak and UV-vis absorption are shift to lower wavelength, indicative of a partial substitution of FA^+ with MA^+ in $FAPbI_3$.[6] The optical bandgap of 0 mol%, 10 mol%, 20 mol%, 30 mol% and 40 mol% are 1.527 eV, 1.539 eV, 1.545 eV, 1.539 eV and 1.539 eV, respectively. PL peak is shift from 818 nm to 802 nm with MACl addition. However, it is noted that the EQE onset edge position is observed at about 840 nm regardless of MACl content (Figure S2d).

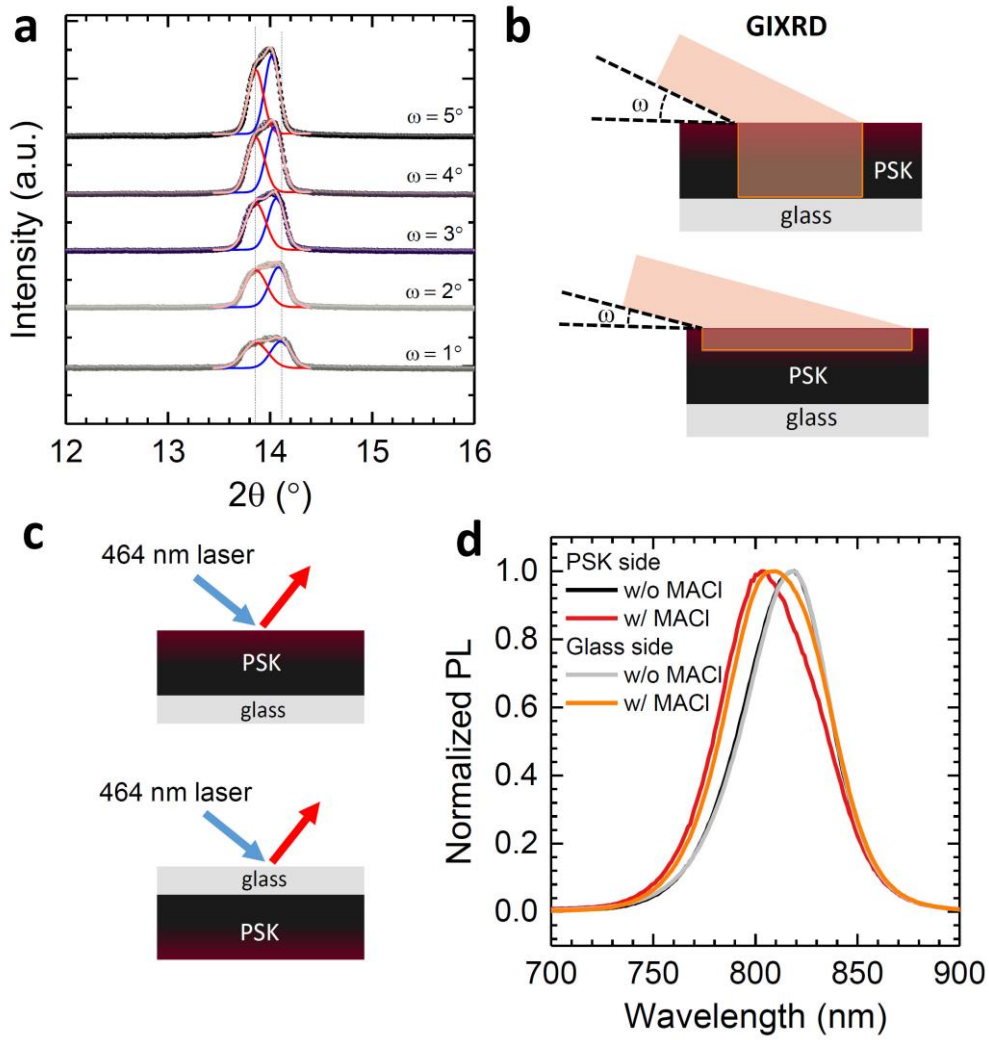

Figure S3. (a) grazing incidence X-ray diffraction (GIXRD) of the perovskite film measured with different incidence angle from 1° to 5°. (b) Schematic representation of the GIXRD geometry. ω is an incidence angle, where the detected depth is deeper if ω is larger. (c) Schematic representation showing laser incident on the perovskite (PSK) side and the glass side. The excitation wavelength was 464 nm. (d) Steady-state PL of the perovskite films based on the annealed $FAPbI_3$ formed from the synthesized $FAPbI_3$ powder without and with 20 mol% MACl.

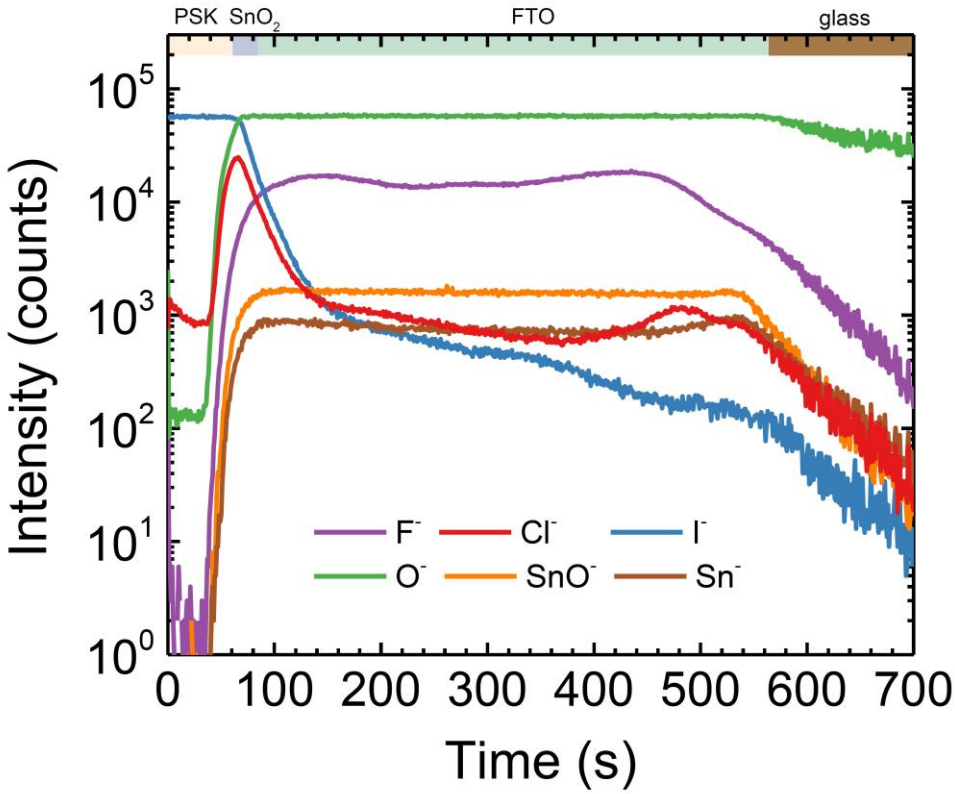

Figure S4. Time-of-flight secondary ion mass spectroscopy (TOF-SIMS) profiles of the perovskite film based on the synthesized $FAPbI_3$ powder with 20 mol% MACl. Depth profiling was performed from the perovskite layer to the FTO substrate in negative polarity.

Note for Figure S3 and S4. Regarding the reason for the unchanged onset wavelength of EQE and the change in PL peaks depending on MACl content in Figure S2, we have speculated that this difference might be related to difference in composition along the film depth. Figure S3a shows the grazing incidence angle (ω)-dependent XRD patterns of the annealed $FAPbI_3$ film formed from the synthesized powder with 20 mol% MACl, where the depth in perovskite film can be increased with ω as illustrated in Figure S3b.[7] The penetration depth $\tau_{1/e}$ of $FAPbI_3$ under incidence angle of 1°, 2°, 3°, 4°and 5° are 172.7 nm, 345.3 nm, 517.9 nm, 690.2 nm and 862.4 nm, respectively. As shown in Figure S3a and S3b, the (100) peak is deconvoluted into two peaks at 13.86° (red color) and at ~14.0° (blue color). The detailed parameters are summarized in the Table S1. The red peak corresponds to $FAPbI_3$ but the blue peak might be related to incorporation of smaller MA in the larger FA site. The peak position at 13.86° is unchanged with increasing ω, however, another peak (blue color) shifts from 14.10° to 14.02°. In addition, the peak area ratio of red to blue is increased from 0.88 to 1.18 as the incidence angle is increased from 1° to 5°. This indicates that the underlying MA-incorporated phase is probably located on the surface of the film rather than on the bottom of the film. The full width at half maximum (FWHM) is decreased with increasing ω, which underlines that the $FAPbI_3$ perovskite grain size is

increased going from top surface to the bulk film. From the PL measurement illuminated on different side in Figure S3c, no change in PL emission peak position is observed regardless of illumination side for the $FAPbI_3$ film without MACl (Figure S3d). On the other hands, a slight change in PL peak position is observed for the 20 mol% MACl case, where the glass side illumination results in PL emission at a slightly longer wavelength, which is indicative of difference in composition between top and bottom of the film. According to GIXRD and illumination-side-dependent PL, MACl assists to increase grain size of $FAPbI_3$ and exists near the surface of $FAPbI_3$ rather than incorporation into bulk $FAPbI_3$, which can explain the reason why the onset wavelength in EQE together with the (100) peak position in XRD were unchanged with MACl. We also measured time-of-flight secondary ion mass spectroscopy (TOF-SIMS) to investigate the position of residual Cl inside the film. As shown in Figure S4, due to MA cation located near perovskite surface, the Cl content decreases going from the top to the bottom in the perovskite layer. However, the Cl content sharply increases when approaching the SnO_2 layer, which indicates that most of Cl is located near SnO_2 layer and this location of Cl was reported to improve stability.[8]

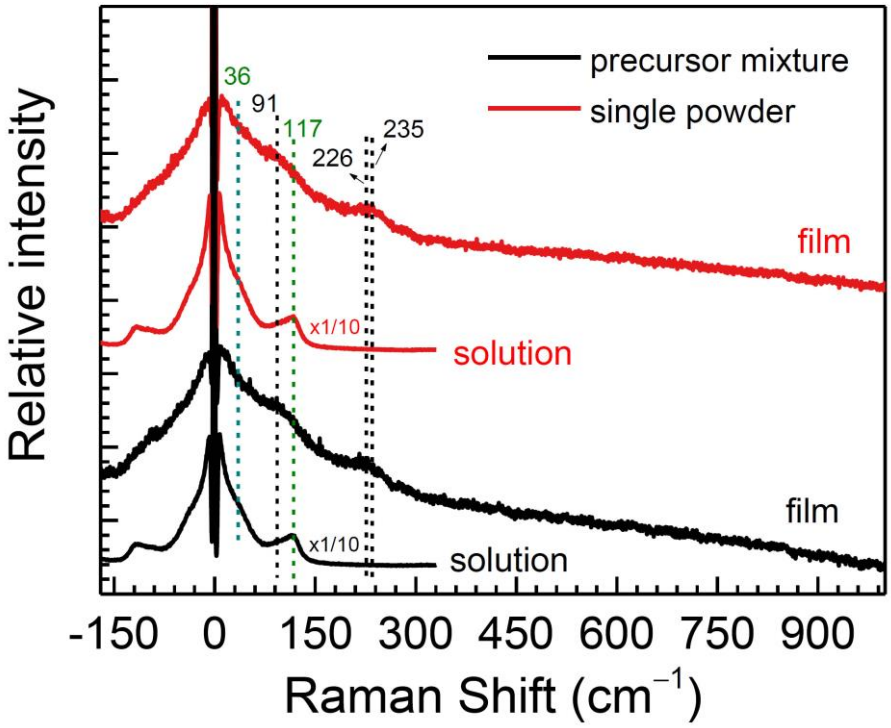

Figure S5. Raman spectra of solutions and films based on the conventional precursor mixture and the synthesized $FAPbI_3$ powder.

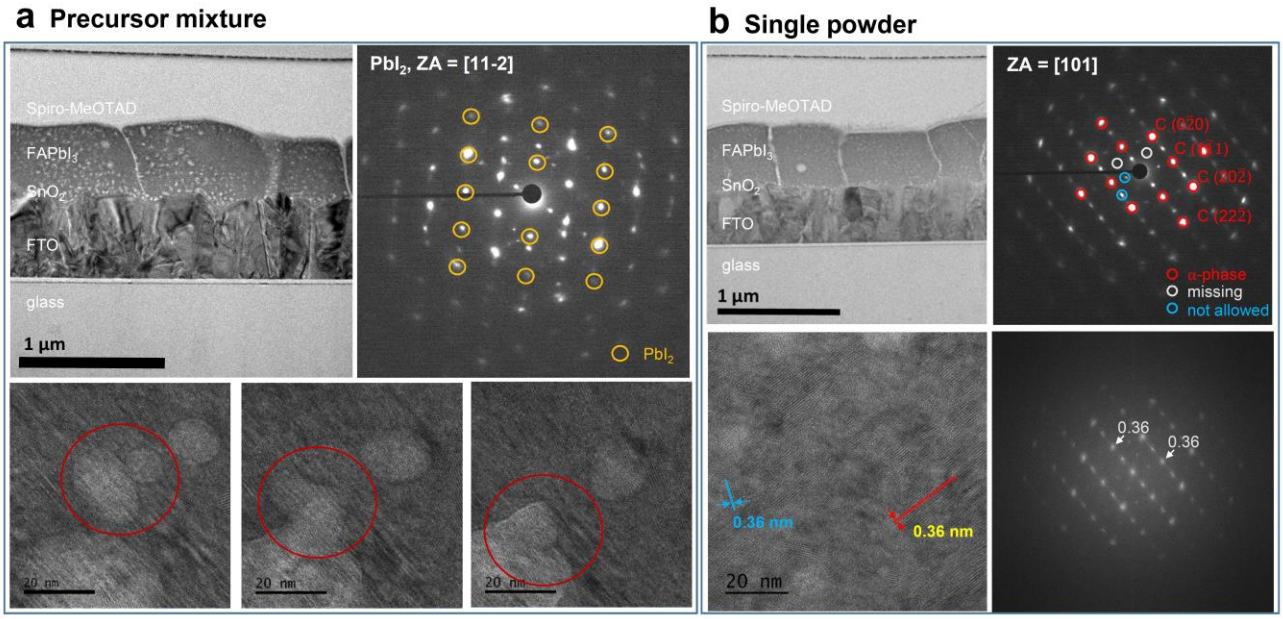

Figure S6. Transmission electron microscopy (TEM) images of cross-section of the device based on powder precursor and conventional precursor. (a) Cross-sectional TEM bright field image (Top left) with a selected area electron diffraction (SAED) pattern (Top right) showing clear refraction spots corresponding to PbI_2 in yellow circles of $FAPbI_3$ prepared by conventional solution spin coating method. Series high resolution TEM images (bottom three) showed unidentified pores in the films moving progressively during observation in the microscope. (b) Cross-sectional TEM bright field image (Top left) with a SAED pattern (Top right) showing cubic α-phase diffraction spots in red circles along with not-allowed spots in blue circles (Top right) of a $FAPbI_3$ film prepared by powder precursor method. High resolution TEM lattice image (bottom left) with corresponding Fast Fourier Transform (FFT) pattern (bottom right).

Note for Figure S6. Structural property of both $FAPbI_3$-based perovskite solar cells prepared using the conventional precursor mixture and the synthesized powder was investigated by TEM. Cross-sectional TEM bright field image (top left) with a selected area electron diffraction (SAED) pattern (Top right) showing clear reflection spots corresponding to PbI_2 (PDF card no.: 00-007-0235) in yellow circles of the $FAPbI_3$-based cell prepared by the conventional precursor mixture shown in Figure S6a. Besides the diffraction spots matched with PbI_2 in yellow circles, all the extra spots are, un-identified though, clearly diffracted from twice larger interplanar spacing than PbI_2. Rothmann *et al.*[9] suggested that the appearance of forbidden reflections indicating an unidentified phase formed during degradation under electron beam irradiation (in their case, $MAPbI_3$). The final by-product of

degradation in $MAPbI_3$ and also $FAPbI_3$ would be PbI_2, although different mechanisms. Until now the exact degradation route is not identified. With e-beam irradiation, volatile molecules are removed from perovskites in an ordered fashion, then the intermediate phases with the same orientation with both PbI_2 and $FAPbI_3$ phases can be found, as shown in SAED in Figure S6a (top right figure). A series of high resolution TEM images (bottom three) show unidentified pores in the films moving progressively during observation in the microscope. The observed and moving pores are speculated as an intermediated phase during degradation under e-beam irradiation. Many more pores in the conventional precursor-mixture-based $FAPbI_3$ films were often found. With almost the same TEM-specimen preparation procedures including careful FIB milling and quick and low-dose TEM observation for both the $FAPbI_3$ cells, the conventional precursor mixture ones showed already in the middle of degradation, without observing the α-$FAPbI_3$ phase at all. Figure S6b shows cross-sectional TEM bright field image (top left) with a SAED pattern (top right) showing cubic α-phase diffraction spots in red circles along with not-allowed spots in blue circles of a $FAPbI_3$ film prepared by the synthesized powder. The SAED pattern (top right in Figure S6b) is matched with cubic phase of $FAPbI_3$[10] and/or close to trigonal perovskite phase of $FAPbI_3$ (P3m1 space group, α-phase).[11] It is not clear that some of not-allowed diffraction spots are found as in blue circles and allowed refraction spots are absent as shown in Figure S6b (top right as in white circles). High resolution TEM lattice image (bottom left) with the corresponding Fast Fourier Transform (FFT) pattern (bottom right) confirms also α-phase of $FAPbI_3$ with cubic (111) interplanar spacing of 0.36 nm. Presence of sub-grains with different orientations (see, blue and red lines in bottom left of Figure S6b) in a large grain is observed. According to TEM observations, the synthesized powder-based $FAPbI_3$ film in the device contains cubic perovskite α-phases without any sign of degradation and no trace amount of PbI_2. The cells could be much more stable in α-phase of $FAPbI_3$ with a smaller number of defects.

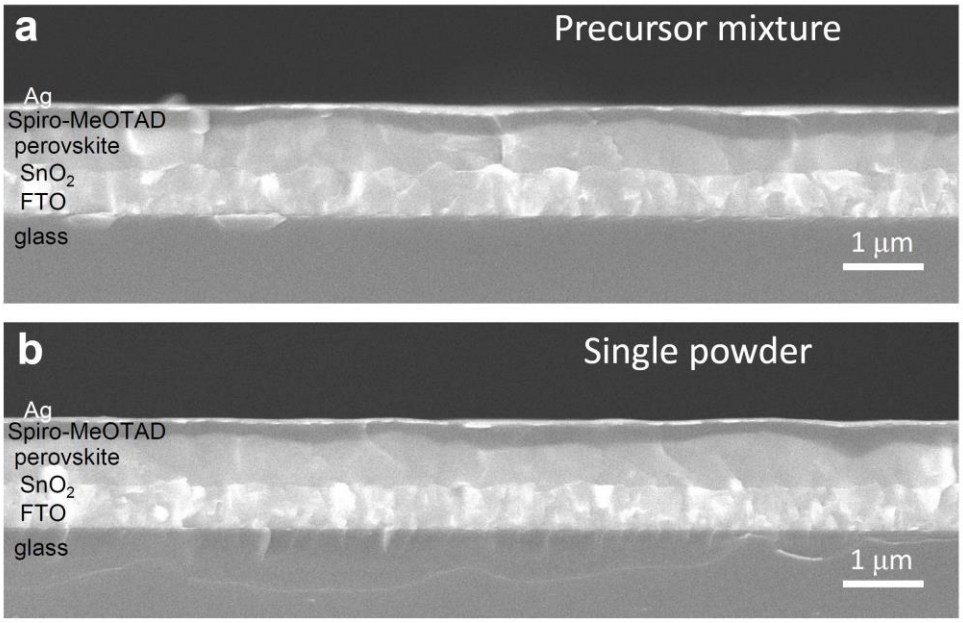

Figure S7. Cross-section image of PSCs with the $FAPbI_3$ perovskite layer formed from (a) the conventional precursor mixture and (b) the synthesized powder.

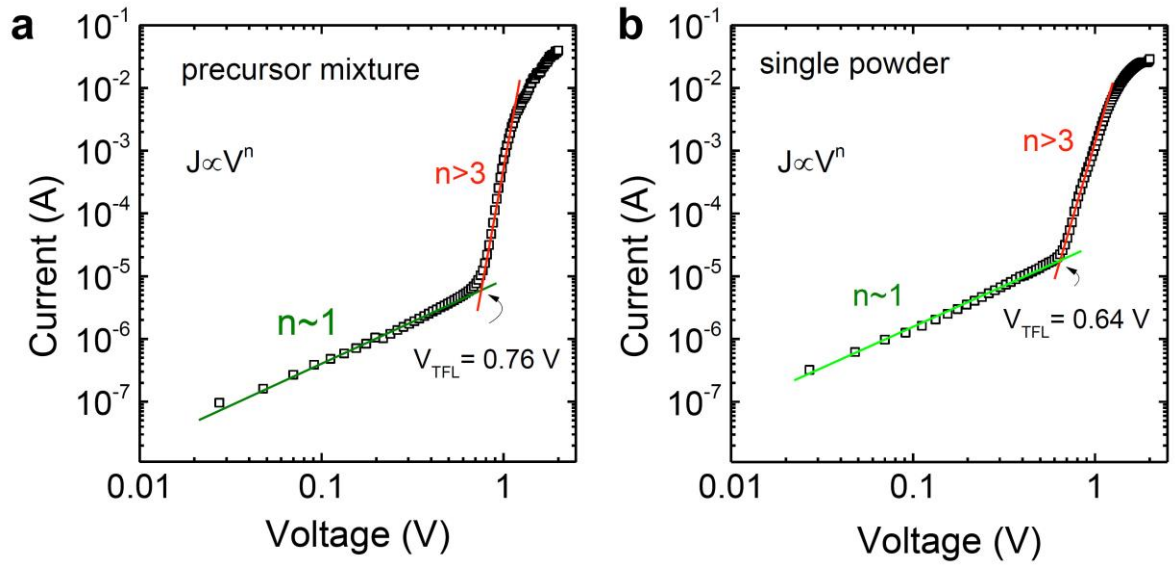

Figure S8. Dark current-voltage of the hole-only devices with the structure of FTO/PEDOT:PSS/perovskite/spiro-MeOTAD/Au based on (a) precursor mixture and (b) single powder.

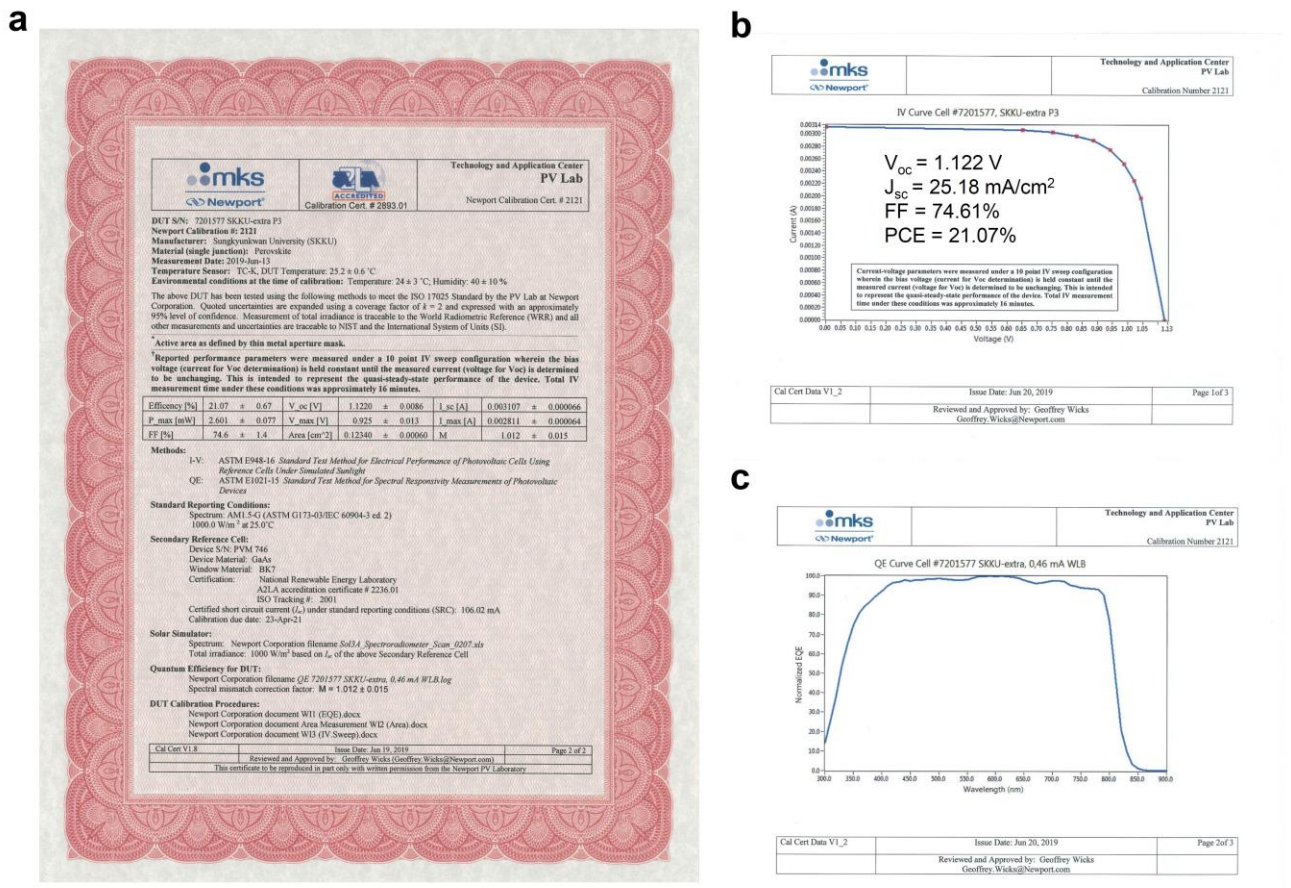

Figure S9. Certificated results from the Newport as a proxy for National Renewable Energy Laboratory (NREL). (a) The certificate of the perovskite solar cell based on the synthesized $FAPbI_3$ powder. The photovoltaic parameters are summarized in the table on the certificate with the PCE of 21.07%. The area of aperture mask is 0.1234 cm^2. The device was measured without encapsulation. (b) The certificate I-V curve with V_{oc} of 1.122 V, J_{sc} of 25.18 mA/cm^2, FF of 74.61% and PCE of 21.07% obtained by the quasi-steady-state measurement to show the stable and reliable performance. (c) Normalized EQE measured under a white light bias. The EQE was measured to verify linearity of operation and determine spectral correction factor.

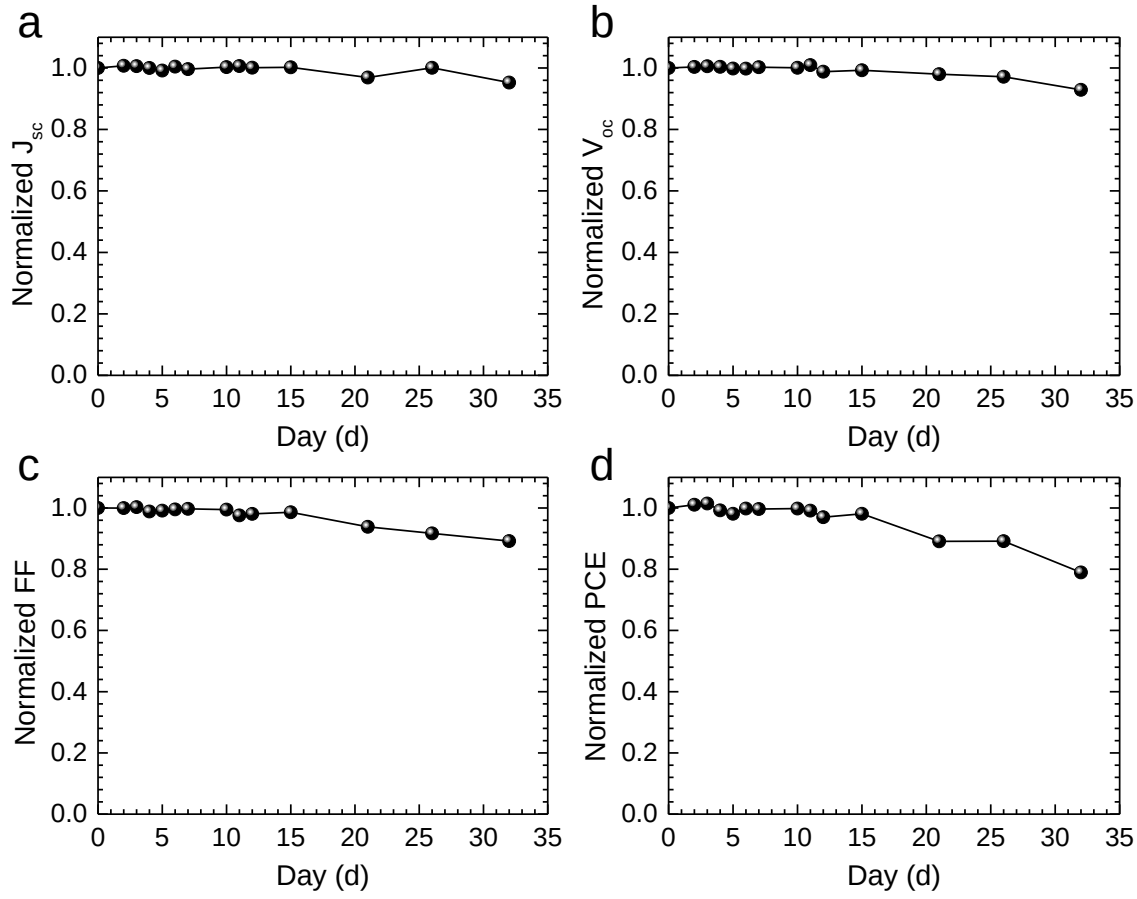

Figure S10. (a-d) Normalized photovoltaic parameters as a function of time to determine that stability of PSCs based on the synthesized $FAPbI_3$ powder. The initial PCE of the device was 20.95% with J_{sc} of 23.89 mA/cm^2, V_{oc} of 1.11 V, FF of 0.79. The devices were stored in the desiccator in the dark under the relative humidity of 10% - 20%. The relative humidity of the J-V measurement condition was around 20%-50%. The device performance was recorded using the reverse scan at scan rate of 130 mV/s.

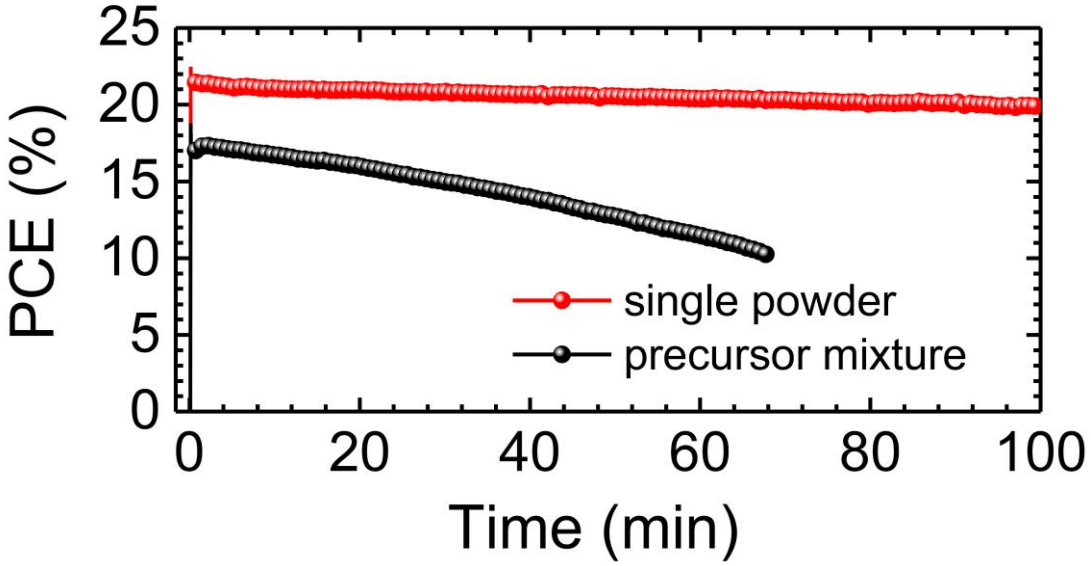

Figure S11. PCEs as a function of time under continuous one sun illumination in ambient condition (relative humidity of about 30%). PCE was monitored at maximum power point using the unencapsulated devices.

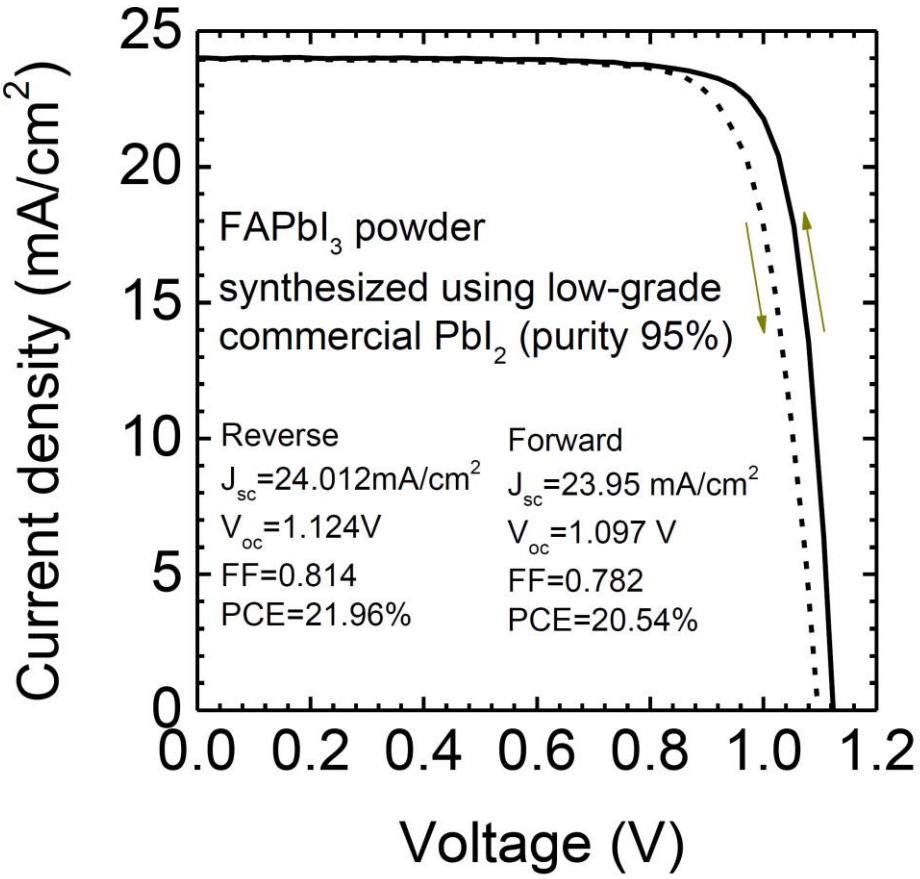

Figure S12. Reverse and forward scanned J-V curves of PSC based on the $FAPbI_3$ powder synthesized using a commercial low-grade (95%) PbI_2. The scan rate was 130 mV/s.

Table S1. The summary of the fitted XRD peak under different incidence angle.

Incidence angle (°)	Peak position (°)	Peak Height (a.u.)	Integrated area (a.u.)	FWHM (°)
5	14.02	6792.30	1220.08	0.17
	13.86	5535.42	1031.59	0.18
4	14.04	5647.32	1124.44	0.19
	13.86	4757.40	1016.00	0.20
3	14.05	4457.54	941.36	0.20
	13.86	4047.02	991.25	0.23
2	14.08	3446.87	785.78	0.21
	13.86	3201.81	862.88	0.25
1	14.10	2303.72	581.59	0.24
	13.86	2196.20	664.40	0.28

Table S2. TRPL fitting results obtained using bi-exponential decay equation $y = y_0 + A_1\exp(-(x-x_0)/\tau_1) + A_2\exp(-(x-x_0)/\tau_2)$, in which τ_1 is time constant for fast decay component and τ_2 is time constant for slow decay component. Average lifetime was estimated from $\tau_{ave} = (A_1\tau_1^2 + A_2\tau_2^2)/(A_1\tau_1 + A_2\tau_2)$. The excitation wavelength is 375 nm.

films	y_0	x_0	A_1	τ_1 (ns)	A_2	τ_2 (ns)	τ_{ave} (ns)
Precursor mixture	4.13	20.70	777.30	8.75	569.90	152.52	142.09
powder	7.60	20.64	595.08	17.89	723.59	319.47	306.20

Table S3. Photovoltaic parameter of PSCs based on the synthesized powder and the precursor mixture with the structure of glass/FTO/SnO_2/perovskite/spiro-MeOTAD/Ag under AM 1.5G one sun illumination (100 mW/cm^2) at scan rate of 130 mV/s.

Device	Scan direction	J_{sc} (mA/cm^2)	V_{oc} (V)	FF	PCE(%)
Powder	reverse scan	24.148	1.1139	0.8076	21.72
	forward scan	24.113	1.0896	0.7806	20.51
Precursor mixture	reverse scan	23.479	1.0522	0.7234	17.87
	forward scan	23.584	1.0107	0.6774	16.15

Table S4. Capacitance (C), area (A), thickness (d), trap-filled-limit voltage (V_{TFL}), relative dielectric constant (ε), defect density (N_{defect}) of perovskite films based on the synthesized powder and the precursor mixture.

Devices	C (F)	A (cm^2)	d (nm)	V_{TFL} (V)	ε_r	$N_{defects}$ (cm^{-3})
powder	1.34×10^{-8}	0.2034	627.0	0.64	46.7	0.84×10^{16}
precursor mixture	1.36×10^{-8}	0.1985	604.6	0.76	46.8	1.08×10^{16}

Table S5. Scan rate dependent photovoltaic parameter of PSCs based on the precursor mixture with the structure of glass/FTO/SnO_2/perovskite/spiro-MeOTAD/Ag.

Scan rate	Direction[a]	J_{sc} (mA/cm^2)	V_{oc} (V)	FF	PCE(%)
1300 mV/s	RS	23.974	1.0259	0.7438	18.29
	FS	23.986	1.0043	0.7377	17.77
650 mV/s	RS	23.847	1.0227	0.7398	18.04
	FS	23.884	1.0037	0.7335	17.58
130 mV/s	RS	23.635	1.0269	0.7331	17.79
	FS	23.731	1.0048	0.7139	17.02
65 mV/s	RS	23.478	1.0251	0.7289	17.54
	FS	23.627	1.0007	0.6922	16.37
26 mV/s	RS	23.206	1.0279	0.7249	17.29
	FS	23.590	1.0120	0.6510	15.54
13 mV/s	RS	22.910	1.0271	0.7240	17.04
	FS	23.365	1.0130	0.6456	15.28
6.5 mV/s	RS	22.478	1.0297	0.7208	16.68
	FS	23.022	1.0213	0.6466	15.20

[a] Scan direction, RS represent reverse scan and FS represent forward scan.

Table S6. Scan rate dependent photovoltaic parameter of PSCs based on the synthesized powder with the structure of glass/FTO/SnO_2/perovskite/spiro-MeOTAD/Ag.

Scan rate	Direction[a]	J_{sc} (mA/cm^2)	V_{oc} (V)	FF	PCE(%)
1300 mV/s	RS	23.963	1.0954	0.8301	21.79
	FS	23.969	1.0759	0.7942	20.48
650 mV/s	RS	24.075	1.0981	0.8158	21.57
	FS	24.085	1.6960	0.7887	20.32
130 mV/s	RS	23.985	1.1047	0.8120	21.51
	FS	24.030	1.0707	0.7872	20.25
65 mV/s	RS	24.016	1.1075	0.8040	21.39
	FS	24.002	1.0712	0.7813	20.09
26 mV/s	RS	23.989	1.1083	0.7945	21.12
	FS	23.902	1.0674	0.7723	19.70
13 mV/s	RS	23.929	1.1082	0.7832	20.77
	FS	23.902	1.0671	0.7471	19.05
6.5 mV/s	RS	23.852	1.1088	0.7688	20.33
	FS	23.888	1.0589	0.7281	18.42

[a] Scan direction, RS represent reverse scan and FS represent forward scan.

References

1. Birkholz, M.; Fewster, P. F.; Genzel, C., Thin film analysis by X-ray scattering. Wiley-VCH, Weinheim; 2006; p xxii, 356p.
2. Berger, M., XCOM: Photon Cross Sections Database; https://www.nist.gov/pml/xcom-photon-cross-sections-database **2010**.
3. Rose, A. Space-charge-limited Currents in Solids. *Phys. Rev.* **1955**, *97*, 1538−1544.
4. Brus, V. V.; Kyaw, A. K. K.; Maryanchuk, P. D.; Zhang, J. Quantifying Interface States and Bulk Defects in High-efficiency Solution-processed Small-molecule Solar Cells by Impedance and Capacitance Characteristics. *Prog. Photovolt. Res. Appl.* **2015**, *23*, 1526-1535.
5. Zhumekenov, A. A.; Saidaminov, M. I.; Haque, M. A.; Alarousu, E.; Sarmah, S. P.;Murali, B.; Dursun, I.; Miao, X.-H.; Abdelhady, A. L.; Wu, T.; et al. Formamidinium Lead Halide Perovskite Crystals with Unprecedented Long Carrier Dynamics and Diffusion Length. *ACS Energy Lett.* **2016**, *1*, 32-37.
6. Zhang, Y.; Grancini, G.; Feng, Y.; Asiri, A. M.; Nazeeruddin, M. K., Optimization of Stable Quasi-Cubic $FA_xMA_{1-x}PbI_3$ Perovskite Structure for Solar Cells with Efficiency beyond 20%. *ACS Energy Lett.* **2017**, *2*, 802-806.
7. Neerinck, D. G.; Vink, T. J., Depth Profiling of Thin ITO Films by Grazing Incidence X-ray Diffraction. *Thin Solid Films* **1996**, *278*, 12-17.
8. Liu, Z.; Deng, K.; Hu, J.; Li, L., Coagulated SnO_2 Colloids for High-Performance Planar Perovskite Solar Cells With Negligible Hysteresis and Improved Stability. *Angew. Chem. Int. Ed.* **2019**, *58*, 11497–11504
9. Rothmann, M. U.; Li, W.; Zhu, Y.; Liu, A.; Ku, Z.; Bach, U.; Etheridge, J.; Cheng, Y.-B., Structural and Chemical Changes to $CH_3NH_3PbI_3$ Induced by Electron and Gallium Ion Beams. *Adv. Mater.* **2018**, *30*, 1800629.
10. Saidaminov, M. I.; Abdelhady, A. L.; Maculan, G.; Bakr, O. M., Retrograde solubility of formamidinium and methylammonium lead halide perovskites enabling rapid single crystal growth. *Chem. Commun.* **2015**, *51*, 17658-17661.
11. Han, Q.; Bae, S.-H.; Sun, P.; Hsieh, Y.-T.; Yang, Y.; Rim, Y. S.; Zhao, H.; Chen, Q.; Shi, W.; Li, G.; Yang, Y., Single Crystal Formamidinium Lead Iodide ($FAPbI_3$): Insight into the Structural, Optical, and Electrical Properties. *Adv. Mater.* **2016**, *28*, 2253-2258.